Thermoelectric infrared microsensors based on a periodically suspended thermopile integrating nanostructured Ge/SiGe quantum dots superlattice

Katir Ziouche, G. Savelli, Zahia Bougrioua, D. Hauser, P. Lejeune, P.M. Michon, Tuami Lasri, Didier Leclercq

HAL Id: hal-01055042
https://hal.science/hal-01055042

Submitted on 25 May 2022

Thermoelectric infrared microsensors based on a periodically suspended thermopile integrating nanostructured Ge/SiGe quantum dots superlattice

K. Ziouche, G. Savelli, Z. Bougrioua, et al.

View Online   Export Citation   CrossMark

ARTICLES YOU MAY BE INTERESTED IN

CrossMark
click for updates

Thermoelectric infrared microsensors based on a periodically suspended thermopile integrating nanostructured Ge/SiGe quantum dots superlattice

K. Ziouche,[1,a)] G. Savelli,[2] Z. Bougrioua,[1,a)] D. Hauser,[2] P. Lejeune,[1] P.-M. Michon,[2] T. Lasri,[1] and D. Leclercq[1]

[1]*IEMN, Institute of Electronics, Microelectronics and Nanotechnology, CNRS and Lille 1 University,*
F-59652 Villeneuve d'Ascq, France
[2]*CEA, LITEN, Thermoelectricity Laboratory, F-38054 Grenoble, France*

This paper presents an original integration of polycrystalline SiGe-based quantum dots superlattices (QDSL) into Thermoelectric (TE) planar infrared microsensors (μSIR) fabricated using a CMOS technology. The nanostructuration in QDSL results into a considerably reduced thermal conductivity by a factor up to 10 compared to the one of standard polysilicon layers that are usually used for IR sensor applications. A presentation of several TE layers, QDSL and polysilicon, is given before to describe the fabrication of the thermopile-based sensors. The theoretical values of the sensitivity to irradiance of μSIR can be predicted thanks to an analytical model. These findings are used to interpret the experimental measurements versus the nature of the TE layer exploited in the devices. The use of nanostructured QDSL as the main material in μSIR thermopile has brought a sensitivity improvement of about 28% consistent with theoretical predictions. The impact of QDSL low thermal conductivity is damped by the contribution of the thermal conductivity of all the other sub-layers that build up the device. © *2014 AIP Publishing LLC*.
[http://dx.doi.org/10.1063/1.4891020]

I. INTRODUCTION

Numerous articles on thermoelectricity highlight the benefit of nanostructuration in the improvement of the thermoelectric devices performance and particularly of the figure of merit $Z = \alpha^2/(\rho.\lambda)$, where α is the Seebeck coefficient (thermoelectric power), ρ is the electrical resistivity, and λ is the thermal conductivity of the thermoelectric material.[1–4] The use of nanostructures, of low dimensional systems or of nano-composite materials, allows confining the phonon heat transport in quasi-2D, 1D, or even 0D. The thermal conductivity of such materials can be considerably reduced by a factor up to 10 or more compared to the bulk counterpart. It is observed that most of the significant improvements in the figure of merit reported so far are essentially due to this decrease of λ and scarcely to the increase of α or to the reduction of ρ. On the other hand, many studies on the growth of SiGe-based quantum dots superlattices (QDSL) underlined the decrease of the cross-plane thermal conductivity.[5–10] However, few studies showed the integration of such kind of nanostructures into Thermoelectric (TE) devices; actually they related mostly to PbTe-based QDSL devices.[11,12]

In this work, we report on the first integration of polycrystalline SiGe-based QDSL into TE devices and we demonstrate that the nanostructuration of the TE material is compatible with the manufacturing process of such systems. The micro-devices are planar infrared microsensors (μSIR) fabricated in a CMOS technology[13,14] and build up with a symmetrical suspended thermopile that exploits the QDSL in

plane. To the best of our knowledge, this is the first time such a configuration is proposed.

The sensitivity to IR irradiance and the response time of the microsensors are measured and compared to those of standard structures where the thermopile is built up with serially connected polysilicon/Gold thermocouples (TC). These characteristics are a function of the thermal resistance of the whole planar structure and of the thermal conductivity of the embedded TE material.

In the first part of this paper, we describe the different layers that were explored. The fabrication of various planar μSIR integrating polycrystalline QDSL or polysilicon is depicted in a second section. The experimental study of the sensitivity and the response time of the various μSIR is presented in the third section. Finally, in the last section, the improvement brought by QDSL is discussed and, when possible, is correlated to the theoretical prediction based on a numerical modeling of the device.

II. GROWTH AND CHARACTERIZATION OF THERMOELECTRIC LAYERS

The TE layers are elaborated by CVD (Chemical Vapor Deposition) techniques on specific templates composed of SiO_2/SiN_X dielectric bilayers deposited on (100) Silicon substrates (380 μm thick and 3-in. diameter). Two families of polycrystalline thermoelectric materials have been considered. The first one corresponds to n-type polysilicon whereas the second one corresponds to n- or p-type {Ge/SiGe} QDSL, which is a superlattice of $Si_{1-y}Ge_y$ dots in $Si_{1-x}Ge_x$ sub-layers (with $1 > y > x$).

First of all, the SiO_2/SiN_X low-stressed support is formed by the thermal growth of a 0.8 μm oxide layer and

a)Authors to whom correspondence should be addressed. Electronic addresses: katir.ziouche@iemn.univ-lille1.fr and Zahia.bougrioua@iemn.univ-lille1.fr

TABLE I. Definition of the QDSL structures.

QDSL	Period	Doping type	SiGe layer thickness (nm)	Dots thickness (nm)	Dots base width (nm)
QDSL$_1$	15	N	16	10–30	100–300
QDSL$_2$	30	N	16	10–30	100–300
QDSL$_3$	30	N	16	5–15	150–200
QDSL$_4$	30	N	12	5–15	150–200
QDSL$_5$	30	P	16	5–15	150–200

TABLE II. Electrical properties of QDSL and polySi layers.

Sample	Thickness (nm)	Carrier concentration (10^{19} cm^{-3})	Mobility μ (cm^2.V^{-1}.s^{-1})	Electrical resistivity ρ (mΩ.cm)
pSi	610	3.9	10	16
pSi$_R$	570	4.6	20	6.7
QDSL$_1$	470	2.3	9.5	28.6
QDSL$_2$	825	2.6	17.5	13.9
QDSL$_3$	770	3	17.2	12.2
QDSL$_4$	670	1.5	17.1	24.2
QDSL$_5$	780	7.8 (p type)	21.9	3.7

the low pressure chemical vapour deposition (LPCVD) of $0.6\,\mu$m SiN$_x$.

A. Growth of the TE materials

The deposition of sub-micrometer thick polysilicon is carried out by LPCVD at low pressure (100 mTorr) in a TEMPRESS® reactor using diluted silane SiH$_4$ and at a temperature of 700 °C. *In situ* n-type doping is performed by introducing diluted PH$_3$ (1% in H$_2$). Two kinds of polysilicon layers are employed as references in this study: denoted "pSi" for plain polysilicon and "pSi$_R$" for annealed polysilicon. For pSi$_R$, a RTA (Rapid Thermal Annealing) heat treatment of 2 min at 1000 °C is performed to modify and optimize electrical and thermoelectric properties.

The QDSL growth is carried out in a RPCVD (Reduced Pressure CVD) reactor at a constant 10 Torr pressure. This deposition technique has already been described in literature for the growth of superlattices.[15–17] CVD offers high layers quality and a good reproducibility. The growth temperature is fixed at 750 °C for all the QDSL. Flow of H$_2$ carrier gas was set to a fixed value of about ten of standard liters per minute. Pure SiH$_4$ was used as the source of Si and germane (GeH$_4$) diluted at 10% in H$_2$ was employed as the source of Ge. The p-type and n-type doping have been obtained from B$_2$H$_6$ and PH$_3$ precursors diluted in H$_2$, respectively. All of

the QDSL have been made on a 15 nm intrinsic polycrystalline SiGe buffer to favor the nucleation of growth. Germanium stoichiometry in SiGe dots was controlled by energy-dispersive X-ray spectroscopy (EDS). Moreover, layers interfaces and thickness, and nanostructures quality were monitored by SEM (scanning electron microscope) or TEM (transmission electron microscope) analyses. For more details concerning the experimental conditions of growth and structural characterization, see Refs. 8 and 9.

Five kinds of QDSL were investigated in this work. The first one, named QDSL$_1$, is build up with 15 alternations from Si$_{1-x}$Ge$_x$ layers to Si$_{1-y}$Ge$_y$ dots. The other four QDSL layers consist in 30 alternations. QDSL$_3$, QDSL$_4$, and QDSL$_5$ integrate smaller dots than QDSL$_1$ and QDSL$_2$. QDSL$_4$ has the thinnest Si$_x$Ge$_{1-x}$ layer period and QDSL$_5$ is the only p-type nanostructured layer of the study. The Ge content x of Si$_{1-x}$Ge$_x$ layers is about 8% for all QDSL (measured by SIMS, Secondary Ion Mass Spectroscopy). The value of y is not known accurately but was estimated to be around 25% based on EDS analysis. Note that, as the size and the density of dots and the Si$_x$Ge$_{1-x}$ thickness vary between the QDSL, the total Ge content differs from one QDSL to another. All structural characteristics of these five QDSL are summarized in Table I.

B. Thermoelectric characterization

All of the nanostructured layers and polySi reference layers have been electrically characterized using the Van der Paw and Hall Effect methods at room temperature. The measured electrical properties are presented in Table II together with the layers thickness measured by SEM on cross-sections.

The room temperature Seebeck coefficients and the estimated thermal conductivities of all of the layers are summarized in Table III.

The in-plane Seebeck coefficients α of the seven layers were not directly measured on the wafers: those later were entirely used for the processing of μSIR with a dedicated mask that covers the entire wafers. In fact they were extrapolated from the α measured in equivalent layers, grown in the same conditions. The Seebeck samples were $2\,$cm $\times\,2\,$mm rectangular strips (measurement method described in Ref. 18).

The thermal conductivity has been measured by the 3ω method for the first and the three last QDSL layers. This method leads to the determination of the cross plane conductivity. The too high roughness (caused by the size of dots and the high period number) in QDSL$_2$ did not allow measuring precisely its thermal conductivity. It is likely the same

TABLE III. Thermoelectric power and thermal conductivities.

Layers	pSi	pSi$_R$	QDSL1	QDSL2	QDSL3	QDSL4	QDSL5
Thermoelectric power[*] (μV/K)	−225	−190	−170	−170	−180	−210	110
Thermal conductivity[Δ] (W/m/K)	35	35	4.8	5	4.4	3.4	4

[*] average values, $\Delta\alpha/\alpha \sim 10\%$
[Δ] from literature for pSi

as for QDSL$_1$, i.e., around some 5 W/m/K. In all cases, the measured values of λ are consistent with those obtained for similar structures in our previous work.[10] In the case of the polysilicon layers, pSi and pSi$_R$, as their thermal conductivity is too high to be measured by 3ω method, we decided to take the n type pSi value found in the literature[19,20] (even though we anticipate that in annealed pSi layers a slight increase of λ may have occurred because of columnar microstructure modification).

III. DESCRIPTION AND FABRICATION OF THE IR THERMAL MICROSENSORS

A. Design of the IR thermal sensor

The topology of the IR microsensor is given in Fig. 1 and is based on works described in Refs. 14 and 21. It is well suited for miniaturization in the perspective to manufacture sensor arrays for low cost IR cameras. This μSIR structure is designed starting from a balanced arrangement of absorbing and reflecting superficial zones laid on a membrane to circumvent the very high thermal conductivity of silicon substrate which prevents to obtain good performances.[22,23] When the sensor is not irradiated, the absorbing and reflecting areas are kept at the temperature of the ambient atmosphere. When the sensor is irradiated by an IR source, a hot zone is generated under the polyimide absorbent while the temperature of the area located under the gold reflector remains approximately constant. The resulting temperature difference is converted into an electromotive force (e.m.f, Seebeck effect) by a zigzag shaped thermopile, series of thermocouples whose junctions are alternatively laid out under the absorbing and the reflecting areas. The thermopile is made up of a periodically Au plated TE material (Fig. 1(b)).

When the TE material is a QDSL-like layer, one can realise that for this planar microsensor topology, the heat flux is flowing parallel to the superlattice sublayers; so it is
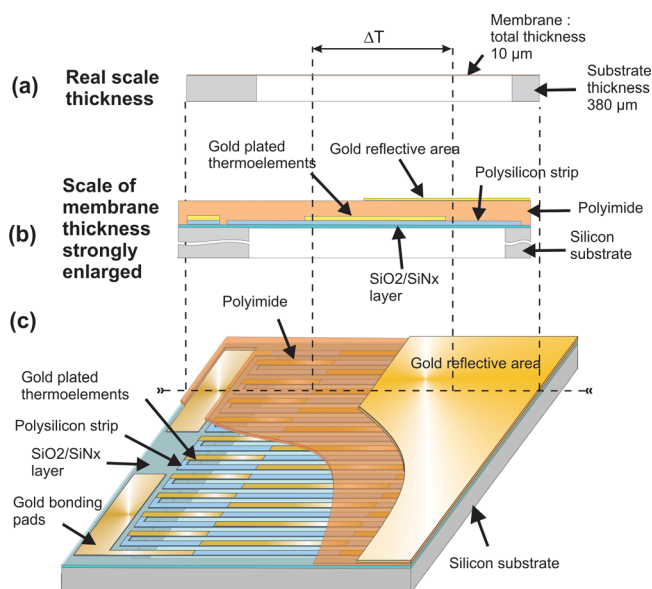
the in plane QDSL properties that counts for the global μSIR behaviour.

Our previous studies have shown that μSIR are more efficient when they are made of a single membrane and of a single reflector.[14] So, such kind of microsensors, with membranes areas of 3×3 mm^2, 3×5 mm^2, and 5×5 mm^2 have been selected for this study. The total number of thermocouples is almost the same for the 3 configurations: N = 52 per sensor for membranes of 3×3 mm^2 and 3×5 mm^2 and N = 50 per sensor for the 5×5 mm^2 membrane. As drawn into Figure 1, the thermopile layout is built up of N/2 strips; each composed of 2 TCs. The total dimensions, including the contact pads and the part of silicon wafer supporting the membrane, lie between 4×4 mm^2 and 5.5×6 mm^2.

On each of the seven wafers several sets of these 3 kinds of sensors were present. A 4th family of sensors corresponding to "distinctive" 5×5 mm^2 μSIR with double-reflecting area was also available (in this case, the TC number is double: N = 100, and they are twice shorter).

B. Fabrication of the sensors

The fabrication of the microsensors requires several processing steps in standard CMOS technology onto the 3 in. wafers described in Sec. II.

Fig. 2(a) shows the schematic of the cross-section of one part of the starting wafer. SiO$_2$/SiN$_x$ low-stressed support sublayers (that will serve as a membrane) cover both side of the Si substrate. The TE layer, pSi or QDSL, was deposited by CVD on the top (see Sec. II A). The first step of the technology is a reactive ion etching of the front side of the wafer, using SF$_6$ and CHF$_3$ mixture gas, in order to form a zigzag shaped strip to realize the thermopile (Fig. 2(b)).

The periodical plating of the thermopile and the bonding pads are processed by lift-off techniques using evaporation of a (Ti(20 nm)/Au(200 nm)) bi-layer (Fig. 2(c)). The absorbing layer is composed of a 10 μm thick photosensitive polyimide resist (HD2731 HDMicrosystems®) spun on the wafer and annealed in a convection furnace with a polymerization annealing cycle (Fig. 2(d)). Contact pads are patterned by UV exposure and stripping. The reflecting area (Fig. 2(e)) is

FIG. 1. Schematic of a single-membrane μSIR: (a) cross section in real scale, (b) cross section along a line of the thermopile strip (membrane thickness enlarged), (c) sight in sectional view.
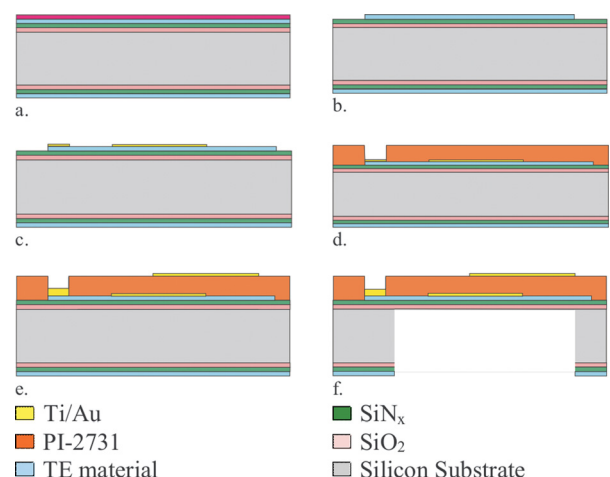

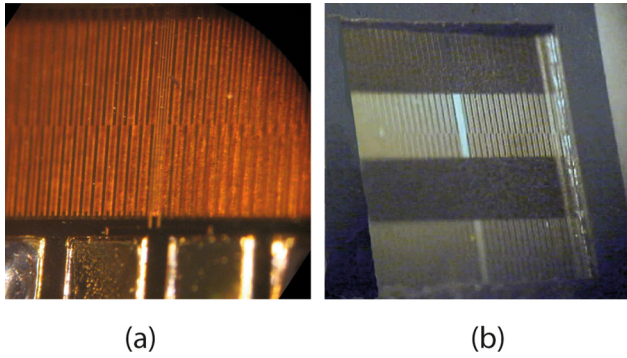FIG. 2. Schematic of the fabrication steps of the microsensor. The TE material is either polySi or QDSL.

FIG. 3. Photographs of microsensors with a single membrane: (a) top view of a 3×3 mm^2 μSIR, (b) backside view of a 5×5 mm^2 μSIR with double reflector.

deposited by evaporation of a (Ti(20 nm)/Au(100 nm)) bi-layer. Finally, the backside is etched to form the sensor membrane by using a STS-ICP equipment (Fig. 2(f)).

Fig. 3 shows the thermopile and the membrane of two typical μSIR.

The internal resistance of the thermopile of each of the fabricated μSIR was measured. Depending on the TE materials used and on the dimension of the μSIR, the values obtained are between 14 kΩ and 180 kΩ and are consistent with the values of the TE layer resistivity and the values of electrical contact resistance.

IV. EXPERIMENTAL CHARACTERIZATION OF THE IR MICROSENSORS

The above described μSIR are designed to be insensitive to the ambient temperature,[14,21] so they do not need any encapsulation during their characterization.

In this article, the two characteristics that we are interested in are the sensitivity of microsensors at irradiance S_E (V/(W/m^2)) and the response time $\tau_{90\%}$ (s), which is the time required for the thermal signal to reach 90% of the steady state in response to a step-like irradiance input.[24] The characterization method has already been described in Ref. 25.

When a microsensor is put in front of an infrared source, the thermopile, which is composed of a doped polysilicon strip (or a doped QDSL strip) periodically covered with gold, generates an e.m.f. that can be expressed by

$$V = N.\alpha.\Delta\theta \qquad (V), \qquad (1)$$

where $\Delta\theta$ (K) is the temperature difference between the hot and the cold junctions; as previously mentioned N is the total number of thermocouples of the thermopile; and α (V/K) is the Seebeck coefficient of each thermocouple.

This voltage depends of the irradiance E (W/m^2) received by the sensor from the IR source and the temperature T_A of the ambient air.

The sensitivity to the irradiance is calculated from the voltage response at ambient temperature

$$S_E = \left(\frac{\partial V}{\partial E}\right)_{T_A=Cste} \quad (V/(W/m^2)). \qquad (2)$$

A home-made characterization set-up has been developed to determine this sensitivity. It is built up with two plates as shown in Fig. 4(a). The sensor is laid on a plate, which is maintained at cold temperature by using a liquid exchanger coupled to a regulated thermostat. The sensor is illuminated by a hot plate target placed at a distance d in front of it.

The temperature of the hot plate T_T can be adjusted from 293 K to 373 K with a PID controller. With such an experimental configuration, the irradiance can be expressed by

$$E = F_{st}.\sigma.\varepsilon_t.T_T^4 \qquad (W/m^2), \qquad (3)$$

where F_{st} is the form factor depending on the distance between the sensor and the hot plate,[26] $\sigma = 5.67 \times 10^{-8}$ (W/m^2/K^4) is the Stefan Boltzmann constant, and ε_t ($\varepsilon_t = 0.97$) is the target emissivity.

The two plates have a total surface by far larger than the microsensor one, so one can assume that this latter is illuminated in quasi influence (F_{st} is close to 1). The thickness d of the air gap (Fig. 4(a)) is equal to 5 cm, the temperature T_A was demonstrated to be independent of the illumination E.[13]

The output voltage V delivered by the μSIR is proportional to the temperature difference $\Delta\theta$ between the junctions of each thermocouple, which itself is proportional to the irradiance E of the hot plate target. The plotting of V versus E leads to a linear trend which slope gives the sensitivity S_E (relation (2)). This is illustrated by the example shown in Fig. 4(b) in the case of 3×3 mm^2 μSIR for the 7 types of TE layers.
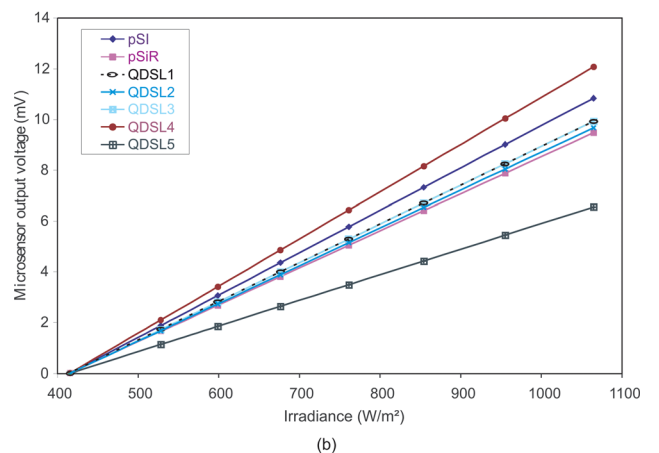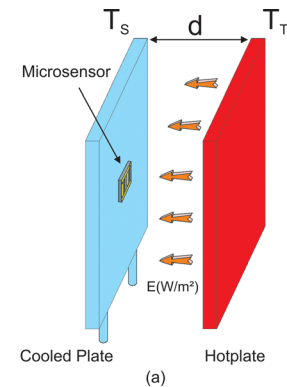

FIG. 4. Characterization of the sensors: (a) Experimental set-up, (b) Experimental output voltages of microsensors with membrane area of 3×3 mm^2 versus irradiance E (W/m^2).

TABLE IV. Sensitivities and response times of the μSIR. (Each value is an average of the experimental values obtained over several identical sensors.)

Layers		pSi	pSi$_R$	QDSL1	QDSL2	QDSL3	QDSL4	QDSL5
μsensor membrane area 3×3 mm^2	Sensitivity (μV/(W/m^2))	15.6	14.6	15.3	14.9	15.3	18.6	10.1
	Response time $\tau_{90\%}$ (ms)	185	172	247	234	213	275	216
Membrane area 3×5 mm^2	Sensitivity (μV/(W/m^2))	17.9	16	*	16.6	13.9	19.7	11.2
	Response time $\tau_{90\%}$ (ms)	202	184	*	208	228	299	243
Membrane area 5×5 mm^2	Sensitivity (μV/(W/m^2))	*	28.2	*	*	25.4	31.2	17.4
	Response time $\tau_{90\%}$ (ms)	*	315	*	*	336	380	329
Membrane area 5×5 mm^2 Double reflector	Sensitivity (μV/(W/m^2))	*	22.2	*	24.2	24.5	27.9	15.3
	Response time $\tau_{90\%}$ (ms)	180	155	*	207	192	221	196

The sensitivities S_E and response times $\tau_{90\%}$ experimentally obtained for the different layers and different configurations of microsensors are given in Table IV.

The missing data « * » (Table IV) correspond to samples for which the characterization was impossible or not reproducible because of some process failure as broken membranes or non-uniform reflectors.

V. DISCUSSION

A. General observations

The experimental results summarized in Table IV show that the changes in the sensitivity and in the response time are related to the nature of the TE layer integrated in the μSIR whatever the dimension of this later. Though significant, there is not a large difference of behavior between μSIR integrating a QDSL and the microsensors integrating polysilicon. For each kind of TE layer, the most sensitive μSIR are those with single reflector and with largest dimension. On the other hand, the μSIR response time follows the trend:

$$\tau_{90\%,\text{5x5 double refl.}} < \tau_{90\%,\text{3x3}} < \tau_{90\%,\text{3x5}} < \tau_{90\%,\text{5x5,single refl}}.$$

For sensors with annealed polySi, compared to standard polySi, it seems that the only gain is a weak improvement of the response time whatever the dimension of the μSIR (-7% to -14%). The irradiance sensitivity is slightly lower for these sensors and this is due to a lower Seebeck coefficient.

The sensors, made of QDSL$_5$ layer, which is the only p-type layer used in this study, have systematically a lower sensitivity. This seems consistent with the fact that it is the most doped QDSL, i.e., with the lowest Seebeck coefficient (Tables II and III).

For the 3×5 mm^2 "extended" membrane μSIR, it is observed that the sensitivity S_E is systematically higher than for 3×3 mm^2 membrane sensors, regardless of the layer used. For the 5×5 mm^2 double reflectors sensors, the sensitivities are systematically lower than their counterparts with single reflector. However, their technological interest lies in their better response times: $\tau_{90\%}$ is reduced almost by half.

The fastest microsensors are those made with the annealed pSi$_R$ layer with a double reflector ($\tau_{90\%} = 155$ ms); while for the same geometry, the slowest are those built with the QDSL$_4$ layer presenting shorter period SL and smaller QD dots ($\tau_{90\%} = 221$ ms).

B. Understanding the μSIR response time

Compared to the sensitivity S_E, the thermal response time $\tau_{90\%}$ is a secondary working parameter of the μSIR but still interesting to understand. Its value is mainly related to the thermal dissipation through the global structure. Its theoretical modeling is possible. Though out of scope of this work, we give hereafter a phenomenological and simplified description of $\tau_{90\%}$ in order to interpret the different behaviors and trends experimentally observed.

If one apply an electrical analogy for each "cell" of a thermopile, i.e., each thermocouple and its proximate medium (membrane, reflector or absorbent…), then the thermal response time of each cell τ_{CELL} is proportional to the product of its thermal resistance and of its heat capacitance

$$\tau_{\text{CELL}} \sim R_{\text{th}}.C_{\text{th}},$$

where $R_{\text{th}} \sim L/(\lambda_{\text{eq}}.e.l)$ and $C_{\text{th}} \sim C.d.L.e.l$; L, e, and l being respectively the length, thickness, and width of a cell; C and d, the specific heat capacity and the density of the cell; and λ_{eq} the cell equivalent thermal conductivity. λ_{eq} integrates 2 parallel contributions: the one of the TE layer (λ_{TE}) and the one of the other sub-layers that build up the TC and its surrounding medium (λ_{around}). Consequently, λ_{eq} can be expressed as

$$\lambda_{\text{eq}} = (e_{\text{TE}}.\lambda_{\text{TE}} + e_{\text{around}}.\lambda_{\text{around}})/e_{\text{eq}}. \quad (4)$$

All these considerations together result in a response time: $\tau_{\text{CELL}} \sim L^2.C.d/\lambda_{\text{eq}}$, where, in order to keep the model simple, we assume that C and d are relatively constant whatever the TE layer, polySi layer, or QDSL.

For a μSIR with a single reflector, as the heat flux is along the x direction (see Fig. 1), the *thermopile* build up with N thermocouples can be considered *equivalent to N/2 strips thermally associated in parallel*. So, the thermal response time of the thermopile is the one of a single strip. As each strip is composed of the 2 TC in series (and their proximate media), this leads to

$$\tau_{90\%} \sim 2.\tau_{\text{CELL}} = 2.L^2.C.d/\lambda_{\text{eq}}. \quad (5)$$

In the case of a *double reflector* μSIR, as there are twice more TC per strip, and as each TC is 2 times shorter, the response time will be half the one for a single reflector μSIR

$$\tau_{90\%,\text{ double refl}} \sim \tau_{90\%,\text{ single refl}}/2.$$

TABLE V. Calculated Sensitivities for $3 \times 3\,\mathrm{mm}^2$ and $5 \times 5\,\mathrm{mm}^2$ μSIR.

Layers	pSi	pSi$_R$	QDSL 1	QDSL 2	QDSL 3	QDSL 4	QDSL 5
Calculated S$_{3 \times 3\,\mathrm{mm}^2}$($\mu$V/(W/m^2))	16,8	14,4	15,1	14,9	15,9	18,7	9,6
Calculated S$_{5 \times 5\,\mathrm{mm}^2}$ (μV/(W/m^2))	32.9	27.9	27.7	27.4	29.2	34.3	17.9

This fully explains one part of the experimental results in Table IV.

As far as $3 \times 3\,\mathrm{mm}^2$ and $5 \times 5\,\mathrm{mm}^2$ single reflector μSIR are concerned, the observed $\tau_{90\%}$ ratio is around 1.4 to 1.8: it is related to the particular design of the Au plating in the TC and should be around 5/3 (not demonstrated in this article).

On the other hand, for the large membrane sensors ($3 \times 5\,\mathrm{mm}^2$), their slower behavior compared to $3 \times 3\,\mathrm{mm}^2$ μSIR is also due to a geometrical effect: it is related to a lower λ_{eq} (lower $\lambda_{\mathrm{around}}$) because of an increased contribution of the membrane to the global thermal resistance.

In the microsensors based on polycrystalline QDSL, as the nanostructuration leads to a reduced thermal conductivity of the TE layer (λ_{TE}), it results into a lower average thermal conductivity in each thermopile cell (λ_{eq}, relation (4)). Owing to relation (5), this leads to a longer response time than in polySi-based μSIR. Experimental results displayed in Table IV show that $\tau_{90\%}$ worsens even more when considering QDSL with even lower thermal conductivity, i.e., with smaller QD and/or smaller SL period. As far as sensors based on the p-type QDSL layer are concerned (QDSL$_5$), $\tau_{90\%}$ is equivalent to the one of sensors based on n-type QDSL$_3$, likely because of an equivalent microstructure.

Incidentally, using the above described phenomenological modelling of $\tau_{90\%}$, one can explain why pSi$_R$-based sensors are slightly faster than their counterpart based on standard polySi (7% to 14% as seen above): it is likely an indirect proof that the RTA annealing has also increased the thermal conductivity of the layer maybe because of an increase of the average diameter of Si columnar crystallites. If one uses relations (5) and (4), this would mean a λ_{TE} increase of at least 7% to 14%. It deserves to be confirmed in further experiments.

C. Modeling of μSIR sensitivity

In order to determine the theoretical values of the sensitivity and to compare them to the experience, we made use of an analytical model that we developed in previous studies. It was used to optimize the structural dimensions of planar IR sensors with a square membrane and to identify the ideal positioning of the TC junctions in order to immunize the microsensor from the ambient air temperature variations. For more details on the principle and the singularities of the modeling, one can refer to the descriptions in Refs. 14 and 21.

The calculation of the sensitivity S$_E$ was made for microsensors with square membrane surface and single reflector, i.e., 3×3 and $5 \times 5\,\mathrm{mm}^2$ μSIR.

First, the theoretical thermal gradients $\Delta\theta$ of the seven kinds of microsensors were evaluated by taking into account the thickness and the thermal conductivity of all the sublayers of the structure, i.e., the TE layers (polySi or QDSL) but also

the bilayer dielectric membrane, the polyimide absorbent, and the gold reflector (Tables II and III; see page 80–81, Ref. 14). For TE thermal conductivity λ, the in-plane values needed were assumed to be the same as the values presented in Table III. Typically, the theoretical thermal gradients $\Delta\theta$ are found to vary between 1.436 and 1.712 K for the $3 \times 3\,\mathrm{mm}^2$ sensor and between 2.924 and 3.266 K for the $5 \times 5\,\mathrm{mm}^2$ sensor.

Then, using $V = N.\alpha.\Delta\theta$ (relation (1)), this led to the determination of the theoretical sensitivities given in Table V.

The calculated sensitivities are quite close to the experimental values presented in Table IV, especially for $3 \times 3\,\mathrm{mm}^2$ devices. For the $5 \times 5\,\mathrm{mm}^2$ microsensors, the slight discrepancy for QDSL$_3$ and QDSL$_4$ (experimental S$_E$ are $\sim$10% lower) is likely due to local heat losses in real devices.

One of the initial interests of this study was to quantify the impact of the drastic reduction of the thermal conductivity of the TE layer on the sensitivity of the microsensors when using QDSL instead of polysilicon. The experimental results show that the reduction of the thermal conductivity by a factor of about 10 between the standard polysilicon layer ($\lambda = 35\,\mathrm{W/m/K}$ and S$_{E,3x3\,\mathrm{mm}^2} = 15.6\,\mu$V/(W/m^2)) and the best QDSL layer, i.e., QDSL$_4$ ($\lambda = 3.4\,\mathrm{W/m/K}$ and S$_{E,3x3\,\mathrm{mm}^2} = 18.6\,\mu$V/(W/m^2)), added to the slight variation of Seebeck coefficient (7%), results in a slight improvement of the sensitivity of the $3 \times 3\,\mathrm{mm}^2$ sensors: 19% increase (10% increase for the $3 \times 5\,\mathrm{mm}^2$ sensors).

As the sensitivity S$_E$ is directly proportional to Seebeck coefficient α, *the ratio S_E/α gives the contribution to S_E improvement brought by the thermal resistance of the **whole structure***. So one can estimate the **improvement of S$_E$ only related to the heat transfer change: it is about 28%**. This moderate increase of sensitivity can clearly be correlated to the relative contribution of the TE layer thermal conductivity (λ_{TE}) to the global thermal conductivity (λ_{eq}) that comprises also the contributions of all the other sublayers that build up the structure of the sensor (metals, dielectrics…, see Eq. (4)).

D. Influence of nanostructuration on device performance

Reducing the size of the dots and of the superlattice period, as it results in higher density of discontinuities in- and cross-plane, certainly reduces the thermal conductivity (in- and cross-plane), but this not necessarily results into any modification of the thermoelectric power, nor of the carrier mobility. Both, α^2/ρ and μ, depend on the microstructure and its imperfections and their improvement requires a significant change in the band structure (density of state). That is likely the reason why there is not a drastic change in the IR sensitivity S$_E$ between, for instance, a 30-periods standard QDSL (QDSL$_2$) and a QDSL with reduced SL period and dot diameter (as QDSL$_4$).

Actually, this study is a good example illustrating that, depending on the application involving a TE material, the classical figure of merit ZT *will be or will not be relevant* for the evaluation of the device performance. In our present case, as α^2/ρ and λ of QDSL$_4$ are respectively 2/3 and 10 times their counterpart in unannealed polySi, the gain on ZT (or any quantity directly proportional to ZT) would have been a factor of almost 6 ($ZT_{polySi} = 2.71 \times 10^{-3}$ and $ZT_{QDSL4} = 1.61 \times 10^{-2}$). However, the gain obtained in μSIR performance is obviously lower because this gain is measured by the irradiance sensitivity: its factor improvement is 1.19 as shown above.

As described in Tables II and III, the nanostructuration by the use of QDSL mainly affects the thermal conductivity λ, not the power factor α^2/ρ, when comparing with bulk material. However, some improvements can also be made to increase the value of the power factor, especially by changing the crystal structure of QDSL: for instance by the use of single-crystalline structures (as the ones described in Refs. 8 and 9 with better defined QDs and no columnar structure) or by changing the nature of the integrated dots using the "nanoparticle-in-alloy" approach.[27] This is partly the reason why we currently work on silicides QDSL growth integrating metallic dots to improve the TE performances.

VI. CONCLUSION

This study presents the original and successful integration of Ge/SiGe quantum dots superlattices QDSL in the manufacture process of planar IR microsensors. In such devices, the TE properties of QDSL are exploited in plane, in a thermopile. Five types of planar μSIR using different polycrystalline QDSL (15 and 30 alternations, different dots sizes, n and p doping) were compared with sensors based on standard polysilicon layers. The results show that a moderate improvement in sensitivity to IR irradiance of the μSIR can be achieved thanks to the reduction of the thermal conductivity in nanostructured QDSL TE layers. As predicted by numerical modeling of the complete sensor, this moderate improvement of the performance is consistent with the fact that the drastic reduction of the thermal conductivity is weighted by the thermal conductivity of the other layers forming the whole structure. The nanostructuration has brought a sensitivity improvement of about 28% for a thermal conductivity reduced by a decade. In parallel, this thermal conductivity reduction naturally results into a slight degradation of the thermal response time.

[1]D. M. Rowe, "General principles and basic considerations," in *Thermoelectrics Handbook, "Macro to Nano,"* edited by D. M. Rowe (CRC Press Inc., 2006), pp. 1.1-1.14.

[2]G. Snyder and E. Toberer, "Complex thermoelectric materials," Nature Mater. **7**, 105–114 (2008).

[3]C. J. Vineis, A. Shakouri, A. Majumdar, and M. G. Kanatzidis, "Nanostructured thermoelectrics: Big efficiency gains from small features," Adv. Mater. **22**, 3970–3980 (2010).

[4]J. P. Heremans, M. S. Dresselhaus, L. E. Bell, and D. T. Morelli, "When thermoelectrics reached the nanoscale," Nat. Nanotechnol. **8**, 471–473 (2013).

[5]J. L. Liu, A. Khitun, K. L. Wang, W. L. Liu, G. Chen, Q. H. Xie, and S. G. Thomas, "Cross-plane thermal conductivity of self-assembled Ge quantum dot superlattices," Phys. Rev. B **67**, 165333 (2003).

[6]A. Bernardi, M. I. Alonso, A. R. Goñi, J. O. Ossó, and M. Garriga, "Density control on self-assembling of Ge islands using carbon-alloyed strained SiGe layers," Appl. Phys. Lett. **89**, 101921 (2006).

[7]M. Larry Lee and R. Venkatasubramanian, "Effect of nanodot areal density and period on thermal conductivity in SiGe/Si nanodot superlattices," Appl. Phys. Lett. **92**, 053112 (2008).

[8]D. Hauser, G. Savelli, M. Plissonnier, L. Montès, and J. Simon, "Growth and electrical properties of doped monocrystalline SiGe-based quantum dot superlattices," in Proceedings of the 8th European Conference of Thermoelectrics, Como Italy, 2010.

[9]D. Hauser, G. Savelli, M. Plissonnier, L. Montès, and J. Simon, "Growth of heavily doped monocrystalline and polycrystalline SiGe-based quantum dot superlattices," Thin Solid Films **520**(13), 4259–4263 (2012).

[10]G. Savelli, D. Hauser, D. Michel, and J. Simon, "Growth, electrical and thermal properties of doped mono and polycrystalline SiGe-based quantum dots superlattices," AIP Conf. Proc. **1449**, 275–278 (2012).

[11]T. C. Harman, P. J. Taylor, M. P. Walsh, and B. E. Laforge, "Quantum dot superlattice thermoelectric materials and devices," Science **297**(5590), 2229–2232 (2002).

[12]T. C. Harman, R. E. Reeder, M. P. Walsh, B. E. LaForge, C. D. Hoyt, and G. W. Turner, "High electrical power density from PbTe-based quantum-dot superlattice unicouple thermoelectric devices," Appl. Phys. Lett. **88**, 243504 (2006).

[13]M. Boutchich, K. Ziouche, M. Ait Hammouda Yala, P. Godts, and D. Leclercq, "Package-free infrared micro sensor using polysilicon thermopile," Sens. Actuators, A **121**, 52–58 (2005).

[14]C. Sion, P. Godts, K. Ziouche, Z. Bougrioua, T. Lasri, and D. Leclercq, "Unpackaged infrared thermoelectric microsensor realised on suspended membrane by silicon technology," Sens. Actuators, A **175**, 78–86 (2012).

[15]S. Bozzo, J.-L. Lazzari, C. Coudreau, A. Ronda, F. Arnaud d'Avitaya, J. Derrien, S. Mesters, B. Hollaender, P. Gergaud, and O. Thomas, "Chemical vapor deposition of silicon–germanium heterostructures," J. Cryst. Growth **216**, 171–184 (2000).

[16]J. M. Hartmann, P. Holliger, F. Laugier, G. Rolland, A. Suhm, T. Ernst, T. Billon, and N. Vulliet, "Growth of SiGe/Si superlattices on silicon-on-insulator substrates for multi-bridge channel field effect transistors," J. Cryst. Growth. **283**, 57–67 (2005).

[17]J. Hållstedt, A. Parent, M. Östling, and H. H. Radamson, "Incorporation of boron in SiGe(C) epitaxial layers grown by reduced pressure chemical vapor deposition," Mater. Sci. Semicond. Process. **8**, 97–101 (2005).

[18]M. Boutchich, K. Ziouche, P. Godts, and D. Leclercq, "Characterisation of phosphorus and boron heavily doped LPCVD polysilicon films in the temperature range 293–373 K," IEEE Electron Device Lett. **23**, 139–141 (2002).

[19]A. D. McConnell, S. Uma, and K. E. Goodson, "Thermal conductivity of doped polysilicon layers," J. Microelectromech. Syst. **10**, 360–369 (2001); L. La Spina *et al.*, "Bulk-micromachined test structure for fast and reliable determination of the lateral thermal conductivity of thin films," J. Microelectromech. Syst. **16**, 675 (2007).

[20]Obviously, the room temperature λ value for a polysilicon layer would vary as a function of the key physical properties that significantly impact phonon scattering: (i) the diameter of the crystallites (density of grain boundaries), (ii) the thickness of the film (for very thin layers, surface and interface roughness scattering), (iii) the concentration and distribution of the doping species (effect of impurity scattering and effectiveness of charge carrier *screening*). As an illustration of these issues, one can read for instance M. von Arx *et al.*, J. Microelectromech. Syst. **9**, 136–145 (2000).

[21]M. Haffar, "Etude et realisation de matrices de microcapteurs infrarouges en technologie silicium pour imagerie basse resolution," Ph.D. Thesis, Lille 1 University, 2007.

[22]H. Baltes, O. Paul, and D. Jaeggi, "Thermal CMOS sensors-an overview," Sens. Update **1**, 121–142 (1996).

[23]F. Völklein and H. Baltes, "Optimization tool for the performance parameters of thermoelectric microsensors," Sens. Actuators, A **36**, 65–71 (1993).

[24]The transient have an exponential evolution with a time constant τ corresponding to the time needed to reach 63,2% of the target value. $\tau_{90\%}$ is some 2,3.τ.

[25]K. Ziouche, P. Godts, Z. Bougrioua, C. Sion, T. Lasri, and D. Leclercq, "Quasi-monolithic heat-flux microsensor based on porous silicon boxes," Sens. Actuators, A **164**, 35–40 (2010).

[26]A. B. De Vrient, *La transmission de la chaleur*, 3rd ed. (G. Morin, Canada, 1992), vol. 2.

[27]N. Mingo, D. Hauser, N. P. Kobayashi, M. Plissonnier, and A. Shakouri, "'Nanoparticle-in-Alloy' approach to efficient thermoelectrics: Silicides in SiGe," Nano Lett. **9**, 711–715 (2009).